Simultaneous Inverse Determination of All Optical Properties of Atmospheric Particles: Improved Results by Using a Realistic Phase Function Approximation

MARKUS DEGÜNTHER

DLR, Institut für Physik der Atmosphäre, Wessling, Germany

GOTTFRIED HÄNEL

Institute of Meteorology and Geophysics, Johann Wolfgang Goethe University, Frankfurt am Main, Germany

(Manuscript received 15 April 1998, in final form 6 October 1999)

ABSTRACT

Through mathematical inversion of photometric data all optical properties of atmospheric particles necessary for radiative transfer calculations are derived simultaneously. These optical properties are the volume phase function, the volume extinction, and the volume absorption coefficient. Additionally, the apparent complex refractive index and the apparent volume fraction of soot within the particles are calculated from the absorption-to-extinction ratio. The phase function of the particles is approximated by a combination of two Henyey–Greenstein functions, one of them governing the forward and the other the backward scattering. This approximation contains only three constants, one for weighting of the two Henyey–Greenstein functions, and two asymmetry parameters. It describes very well the phase functions known from measurements on airborne particles in the entire range of scattering angles from 0° to 180°. Thus the new results can be used not only for climate modeling but also for remote sensing applications. First results from the new method are compiled and discussed.

1. Introduction

Atmospheric particles scatter and absorb solar radiation. Consequently, they influence the energy budget of the atmosphere–earth system. To be able to understand the interaction of radiation with particles their optical properties have to be determined. These properties depend on the compositions, structures, shapes, and sizes of the particles (Levin and Lindberg 1979; Patterson 1981; Bohren and Huffman 1983; Hill et al. 1984; Schuerman et al. 1981; Zerull et al. 1980). Atmospheric particles can be mixtures of many different substances and are subject to conversion by a multitude of chemical reactions and physical processes. Thus their optical properties may vary highly with time and space (Levin and Lindberg 1979; Flowers et al. 1969; Shaw 1980; von Hoyningen-Huene and Raabe 1987). Usually the variations are different for different properties. According to the many sources, reactions, and other processes involved, these variabilities are not well understood and hence cannot be modeled reliably. Because most radiative transfer problems can be solved only if complete sets of the optical properties are available, this makes simultaneous measurements of all optical properties needed for radiative transfer calculations desirable.

Recently Hänel (1994) published complete sets of optical properties that had been taken simultaneously from dried atmospheric particles sampled on Nuclepore filters. The results are the volume extinction and absorption coefficients as well as the asymmetry parameter of a Henyey–Greenstein function that was used to approximate the volume phase function. The aim of the present paper is to improve the phase function approximation allowing the use of the results not only for climate modeling but also for remote sensing applications. Thus the new phase function must approximate well-measured phase functions of airborne particles in the atmosphere (e.g., nephelometric measurements) in the entire range of the scattering angles from 0° to 180°. This is achieved using a composite of two Henyey–Greenstein functions with different asymmetry parameters, one of them governing the forward and the other the backward scattering. The weights for each of these two functions are calculated from one additional parameter.

2. Description of the method

With the method to be presented, optical properties cannot be measured directly. They only can be quan-

Corresponding author address: Dr. Markus Degünther, DLR, Institut für Physik der Atmosphäre, P.O. Box 1116, D-82230 Wessling, Germany.
E-mail: markus.deguenther@dlr.de

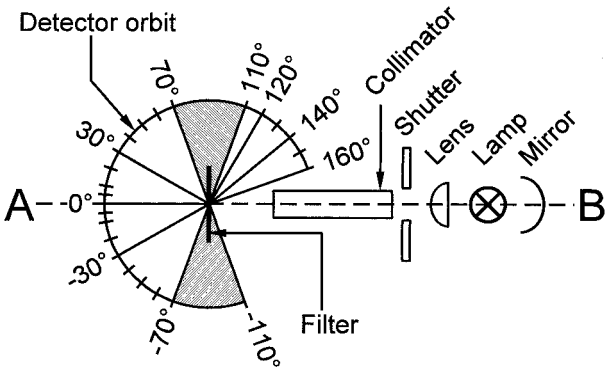

FIG. 1. Schematic illustration of the polar photometer. Normalized signals are measured between −110° and 160° in steps of 10° and at −5° and 5°. Because the very small signals in the hatched ranges are often connected with relative errors exceeding a few percent, these signals are not used during the inversion.

tified indirectly by mathematical inversion of photometric measurements using a suitable radiative transfer model. In this section we describe first the experiment (sampling of particles, the polar photometer, and photometric measurements), second the photometric data to be used for the inversion, third the modeling of these photometric data, and finally the mathematical inversion procedure.

a. The experiment

1) SAMPLING OF PARTICLES

Under specific atmospheric conditions the small-scale variability of the particles' properties may be so large that even results from the ''same'' site but taken with different instruments are difficult to compare. Thus the main goal of our work is not only to obtain complete sets of the particles' optical properties but also to get all of them from the same particles. To achieve this the particles are sampled on Nuclepore filters. Afterward the sample is brought to the laboratory where photometric measurements are performed. Before the measurements it is ensured that the samples are well equilibrated to the laboratory conditions. Thus our results are valid for relative humidities smaller than approximately 30%, which means that they are very close to the optical properties of dry particles (Hänel 1976).

The pore diameters of the filters used are 0.2 μm. This ensures that practically all particles from the filtered air are sampled (Spurný 1965–66; Degünther 1997).

2) POLAR PHOTOMETER

Photometric measurements of the scattered and transmitted (passed without any interaction) radiation are taken from the unloaded and, after sampling, from the particle-loaded filter with the polar photometer by Hänel (1994) (Fig. 1).

In the polar photometer a filter is fixed in a special frame that ensures an even filter surface without any creases. The unloaded filter is illuminated on that side on which, later on, the particles are sampled. The particle-loaded filter is illuminated such that the incoming radiation hits the particles first. This latter precaution ensures the optimum information content about the optical properties of the particles regarding the photometric data from the loaded filter.

A 200-W HMI broadband-radiation lamp is used as radiation source. It provides a spectrum similar to that of extraterrestrial solar radiation. Because the sensitivity of the detector is practically independent of wavelength, the derived optical properties are given as spectral mean values for the extraterrestrial spectrum. They can be used also as spectral values at the wavelength 0.7 μm (Blanchet 1982; Hänel 1994).

For the present work the collimator in the polar photometer had to be improved. After the improvement, at least 99.9% of the incident radiation deviates less than 3.81° from the direction normal to the filter. This allows simpler modeling of the photometric data. For some more details about the polar photometer see Hänel (1994).

b. Photometric data used as dependent quantities during the inversion

For any mathematical inversion, dependent quantities are required that can be (i) measured and (ii) calculated (with a model) from independent quantities. During the inversion procedure those values of the independent quantities are determined, which result in calculated dependent quantities agreeing as well as possible with their measured counterparts.

In our case photometric data from the unloaded and the loaded filter serve as dependent quantities. Independent quantities are the optical properties of the filter, which are derived from the photometric data of the unloaded filter, and the optical properties of the particles, which are derived from the photometric data of the loaded filter. To get the optical properties of the particles the optical properties of the filter must be already known.

One of the prerequisites for the success of the inversion is that the photometric data on the whole have to be sensitive to all optical parameters to be derived. A significant change of one of the parameters should result in a significant change of at least one dependent quantity. This is of special importance, since, for example, we want to get information about the radiation absorption, but we can measure only radiation scattered and transmitted. Second, we want to obtain the parameters describing single scattering, but the photometric data are mainly the result of combined multiple scattering and absorption effects.

In the polar photometer the scattered and transmitted radiation by a filter is measured on a plane perpendicular

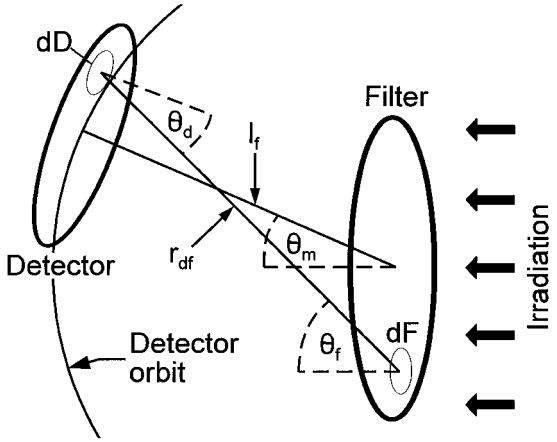

FIG. 2. Illustration of the relevant geometric properties inside the polar photometer used for the calculation of the normalized signal [Eq. (2) in section 2c].

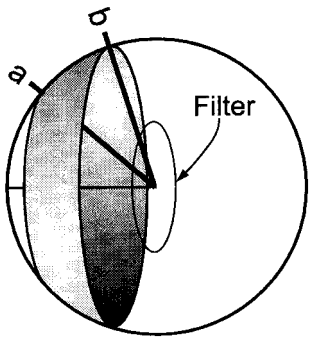

FIG. 3. Illustration of the radiation flux P_{a-b}. The radiation through the gray area is integrated in order to obtain P_{a-b} serving as a dependent quantity.

to the filter at 30 different position angles, between $-110°$ and 160° in steps of 10° and at $-5°$ and 5°. From these signals the photometric data to be used for the inversion are obtained as follows. At first the very small signals at $\pm 80°$, $\pm 90°$, and $\pm 100°$ (from the hatched area in Fig. 1) are excluded from any further consideration because often their relative errors are too large for our purposes. As a further step, the signals at angles with different signs but the same figure are averaged. These results are normalized to the total flux of the incident radiation, which is determined each time before a measurement is taken. From the normalized signals S, five integrals P_{0-30}, P_{30-70}, $P_{110-120}$, $P_{120-140}$, and $P_{140-160}$ are calculated:

$$P_{a-b} = \frac{\pi^2 l_f^2}{90D} \int_{a°}^{b°} S \sin(\theta_m)\, d\theta_m, \tag{1}$$

where l_f is the radius of the circle the detector is moving on, D the area of the detector, S the normalized signal, and θ_m the position angle of the detector in degrees (Fig. 2). As measurements show, the radiation scattered and transmitted by the filter is distributed symmetric with respect to the axis A–B (Fig. 1). Thus, P_{a-b} describes the normalized radiation flux through the surface of a sphere bounded by the latitudes a and b (Fig. 3).

The five normalized fluxes P_{0-30}–$P_{140-160}$ are the dependent quantities used to derive iteratively the optical properties of the filter and the particles. For the calculation of initial values of the optical properties the iteration is starting with, the normalized hemispherical fluxes P_{0-90} and P_{90-180} as well as the normalized signals $S(\theta_m)$ at the position angles 0°, 5°, 10°, 20°, 30°, 140°, 150°, and 160° of the detector have to be additionally used.

Hänel (1994) used for his inversion only the normalized hemispherical fluxes P_{0-90} and P_{90-180} as well as an approximation to the ratio between hemispherical backward and hemispherical forward scattering. For our improved inversion procedure, however, we have to consider normalized signals and nonhemispherical integrals of the normalized signals. For their computation a much more detailed model than that used before had to be developed. This new model shall be outlined next.

c. Modeling of photometric data

The aim of the physical model presented in the following is to describe the dependent quantities with high accuracy. Provided the model would be a bad approximation of reality, good agreement between calculated and measured fluxes could be obtained only if the calculations were based on erroneous optical properties. Thus, without a sufficiently exact radiative transfer model, correct optical properties cannot be found.

1) MODELING OF NORMALIZED DETECTOR SIGNALS

The basic property for our considerations is the normalized detector signal S as a function of the detector's position angle θ_m and the optical properties, the latter represented by the vector $\mathbf{x}$. In general, scattered and transmitted radiation contribute to the signal. However, because of the polar photometer's design, the contribution by the transmitted radiation is restricted to detector position angles between $-13°$ and 13°. The normalized signal reads

$$S(\theta_m, \mathbf{x}) = \frac{\int_F \int_D HN^*(\theta_m, \mathbf{x}) \dfrac{\cos[\theta_d(\theta_m)] \cos[\theta_f(\theta_m)]}{r_{df}^2(\theta_m)}\, dD\, dF}{\int_F H\, dF} + T(\theta_m, \tau), \tag{2}$$

where F is the illuminated part of the filter surface; H the flux density of the radiation incident on surface element dF on the filter; N^* the intensity of scattered radiation by H normalized flowing from dF to surface

element dD on the detector; r_{df} the distance between dF and dD; and θ_d (θ_f) the angle between the line connecting dF and dD and the normal to the detector and filter surface, respectively (Fig. 2). Here, $T(\theta_m, \tau)$ is the part of the normalized signal S that is caused by transmitted radiation. It is calculated from the normalized signal of the incident radiation at θ_m, measured without inserted filter, and the transmission factor according to the Bouguer–Lambert law.

Some important details for modeling are the following.

1) From measurements the flux density H of the irradiation is known as a function of position on the illuminated part of the filter surface. It was found to be symmetric with respect to the vertical and to the horizontal through the center of the filter. Therefore it suffices to model the distribution of H on only one quarter of the filter surface.
2) Since 99.9% of the incident radiation deviates less than 3.81° from the direction normal to the filter, calculations assuming perpendicular incident radiation yield negligible errors only.
3) In the case of no particle loading, **x** contains only the optical properties of the filter [optical thickness, single scattering albedo (ratio of scattering and extinction coefficients = unity minus ratio of absorption and extinction coefficients), and phase function]. Since nearly all collected particles stay on the filter surface, the particle-loaded filter can be treated as a two-layered system in which the optical properties of the filter layer remain unchanged. Thus, if a particle-loaded filter is considered, **x** contains both the optical properties of the unloaded filter and those of the particle layer. Because the optical properties of the unloaded filter are already known, only the optical properties of the particles remain as unknowns in Eq. (2).
4) In the photometer the filter is fixed in a special frame and becomes even without any creases. Its thickness is in the order of 10–20 μm, whereas its extension perpendicular to the incident radiation is about 30 mm. Consequently, the unloaded and loaded filters are treated as media with plane-parallel boundaries and infinite lateral extension.
5) The polarization of radiation needs not be considered (Hovenier 1971; Hansen 1971).
6) The filter and the particle layer both can be regarded as optically homogeneous. Thus the intensity N^* of the scattered radiation may be calculated using the principles of invariance (Chandrasekhar 1960; Hänel 1994).

2) Modeling of phase functions

Finally the phase functions of the particles and the filter have to be specified.

(i) Particles

In the polar photometer, we have scattering of radiation from the solar spectrum by (almost) dry atmospheric particles. The particles contributing most to the scattered radiation have sizes comparable to the wavelengths of solar radiation. They are inhomogeneous agglomerates of different substances and irregular in structure and shape. Therefore the particles' phase function cannot be derived on the basis of already existing radiation scattering theories (e.g., Bohren and Huffman 1983; Yeh and Mei 1980; Bohren and Singham 1991; Liou and Takano 1994): The relevant particles are too large to apply the Rayleigh theory, too small for the geometrical optics theory, and too inhomogeneous and irregular for the Mie and related theories. A method able to describe radiation scattering by arbitrarily structured and shaped particles is that originally proposed by Purcell and Pennypacker (1973). But this method is only applicable to rather small particles, and the required information about the size, structure, shape, and composition of each particle is not available.

Since reliable phase function modeling on a theoretical basis is impossible at present, we found it advantageous to describe the phase function with an empirical formula being able to approximate convincingly the results of measurements for the different types of atmospheric particles.

Many different empirical phase functions have been proposed (e.g., van de Hulst 1980). Among them, the subsequent combination of two Henyey–Greenstein functions is suitable for our purposes:

$$\varphi(\psi) = b\varphi_{\mathrm{HG}}(\psi, g_1) + (1 - b)\varphi_{\mathrm{HG}}(\psi, g_2), \quad (3)$$

where ψ denotes the scattering angle and φ_{HG} a Henyey–Greenstein function defined as

$$\varphi_{\mathrm{HG}}(\psi, g_i) = \frac{1 - g_i^2}{[1 + g_i^2 - 2g_i \cos(\psi)]^{3/2}},$$

where g_i is the asymmetry parameter of $\varphi_{\mathrm{HG}}(\psi, g_i)$ and $g = bg_1 + (1 - b)g_2$ the asymmetry parameter of $\varphi(\psi)$. Formulations similar to Eq. (3) are frequently used in the literature (Irvine 1965; Kattawar 1975; Durkee et al. 1991; Wang and Gordon 1993; McGuire and Hapke 1995). With the above phase function $\varphi(\psi)$, measurements on airborne particles can be approximated very well since one Henyey–Greenstein function suffices to describe realistically either the forward or the backward scattering alone and in Eq. (3) the forward and backward scattering is determined nearly exclusively by $\varphi_{\mathrm{HG}}(\psi, g_1)$ and $\varphi_{\mathrm{HG}}(\psi, g_2)$, respectively. Regarding the mathematical inversion, it is a big advantage that, using Eq. (3), the forward and backward scattering may be varied nearly independently from each other.

(ii) Filter

The phase function of the filter is unknown and cannot be measured directly. Thus we searched for a phase

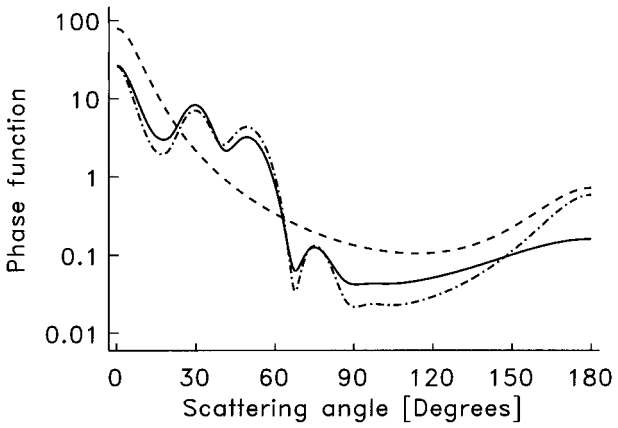

FIG. 4. Filter phase function. The solid and dash-dotted curves represent the variability of the phase functions assigned to the unloaded filters. The dashed curve is added for comparision. It shows a three-parameter combination of two Henyey–Greenstein functions [$g_1 = 0.85$, $g_2 = -0.65$, $b = 0.95$; see Eq. (3)]. The rippled structure of the filter phase functions for scattering angles between 10° and 90° is due to the parameterization. These ripples smooth out since more than 90% of the radiation scattered by the filter is multiple scattered. Thus, the ''effective'' filter phase function is similar to a three-parameter combination of two Henyey–Greenstein functions, but with enhanced values for scattering angles between about 20° and 60°.

function that is consistent with the photometric data from the unloaded filters. This resulted in a phase function of the filter containing two Henyey–Greenstein functions like in the particle case with some additional functions enhancing forward scattering mainly in the range of scattering angles from 20° to 60° (Fig. 4). For details see Degünther (1997).

3) CALCULATION OF PHOTOMETRIC DATA

During the mathematical inversion calculated and measured photometric data have to be compared. The basis of the calculations is Eq. (2), where the normalized intensity N^* of the scattered radiation and the flux density H of the incident radiation must be known as functions of the optical properties and of the position on the filter, respectively. To get N^* as function of the optical properties, radiative transfer calculations are performed on the basis of the principles of invariance (Hansen 1969), which in vector and matrix notation are also known as the adding method (van de Hulst 1980). The details of the method have been already described by Hänel (1994).

From photometric measurements carried out without filter the distribution of the flux density H of the radiation incident on the filter can be approximated by a simple model (Degünther 1997). Tests showed that uncertainties of the photometric data used for the mathematical inversion caused by this irradiation model are small. They are at maximum less than 10% of the sum of all experimental errors.

After determining N^* and H, the normalized signals are calculated using Eq. (2). Finally, these signals inserted in Eq. (1) lead to the five normalized fluxes P_{0-30}–$P_{140-160}$ being the dependent quantities.

It will be shown in section 3 that our entire model for the normalized signal S [Eq. (2)] and for the normalized fluxes P_{a-b} [Eq. (1)] is of the required high accuracy.

d. Mathematical inversion procedure

The aim of the inversion procedure is to determine values of the optical properties (independent quantities) yielding ''best agreement'' between calculated and measured photometric data (dependent quantities). The inversion is based on the following system of nonlinear equations describing the differences between the results of calculation and measurement:

$$G_{0-30}[P_{0-30,m} - P_{0-30}(\mathbf{x})] = \Delta_1(\mathbf{x})$$

$$\vdots$$

$$G_{140-160}[P_{140-160,m} - P_{140-160}(\mathbf{x})] = \Delta_5(\mathbf{x}). \qquad (4)$$

The $P_{a-b,m}$ and $P_{a-b}(\mathbf{x})$ denote the measured and calculated radiation fluxes for the particle-free or the particle-loaded filter, and the G_{a-b} $(=P^{-1}_{a-b,m})$ are weights that ensure that the values of Δ_1–Δ_5 all are principally of about the same order of magnitude. Best agreement is reached when the sum over the squares of Δ_1–Δ_5 is minimum. Hence, the aim of the inversion procedure is to find the optical properties $\mathbf{x}$ fulfilling:

$$\sum_{i=1}^{5} \Delta_i^2(\vec{\mathrm{x}}) = \text{minimum for all } \mathbf{x} \text{ of } \mathbf{Y}. \qquad (5)$$

The set $\mathbf{Y}$ contains all physically meaningful combinations of optical properties. To find the vector $\mathbf{x}$ fulfilling Eq. (5), the system of nonlinear equations Eq. (4) has to be solved. For this, it is linearized and the solution is found iteratively using the Newton scheme. For solving the linearized system during each iteration step, the singular value decomposition (SVD) (Press et al. 1992) is applied. This technique has two great advantages. First it is able to find physically meaningful answers even if the set of equations is ill conditioned or singular (Press et al. 1992). Second, even if there does not exist an exact solution, SVD will find an approximate one (Press et al. 1992). The iteration will be finished if, after an iteration step, the agreement between weighted calculated and measured radiation fluxes is improved by less than 10^{-5}.

During the development of the inversion procedure, it became clear that an iteration only can succeed if it starts with values of the optical properties already approximating well the final results. Thus, the main difficulty is to find such starting values. This problem is solved in two parts. First step: As optical thickness and single scattering albedo, the final results of the inversion procedure by Hänel (1994) are chosen. Next we cal-

TABLE 1. Outline of the systems of nonlinear equations used in the indicated order to find starting values for the final iteration. These systems are solved iteratively for the variables in the first column applying a damped progress of iteration. This means, during each iteration step the reciprocals of such singular values are set to zero, which are less then the largest singular value times the damping factor given in the right column.

Improved parameters	Photometric data (weights) considered	Damping
ω, b	$P_{120-140}$ ($G_{120-140}$), $P_{140-160}$ ($G_{140-160}$)	10^{-3}
g_2*	$P_{120-140}$ ($G_{120-140}$), $S(140)$ [0.2 $S(140)^{-1}$], $S(150)$ [0.3 $S(150)^{-1}$], $S(160)$ [0.5 $S(160)^{-1}$]	10^{-3}
g_1	P_{0-30} (G_{0-30}), P_{30-70} (G_{30-70}), $P_{110-120}$ ($G_{110-120}$)	10^{-3}
ω	P_{0-30} (G_{0-30}), P_{30-70} (G_{30-70}), $P_{110-120}$ ($G_{110-120}$), $P_{120-140}$ ($G_{120-140}$), $P_{140-160}$ ($G_{140-160}$)	10^{-3}
ω, g_1, b	P_{0-30} (G_{0-30}), P_{30-70} (G_{30-70}), $P_{110-120}$ ($G_{110-120}$), $P_{120-140}$ ($G_{120-140}$), $P_{140-160}$ ($G_{140-160}$)	10^{-3}

* If the iteration for g_2 does not succeed, the photometric data are calculated for different values of g_2. The value that leads to best agreement is chosen.

culate the parameters of our improved phase function [g_1, g_2, and b in Eq. (3)] such that its asymmetry parameter equals that by Hänel (1994). For this $g_2 = -0.55$ and $b = 0.9584$ are assumed according to our experience, and g_1 is calculated from the expression for g [see 2c(2)]. Second step: These values are improved. Our way of finding improved values is to improve not all the five parameters at the same time. We first consider exclusively those to which the photometric data are most sensitive. Only if these parameters are improved sufficiently can we start changing the parameters with less influence. To realize this way of finding starting values several specific systems of nonlinear equations similar to Eq. (4) are formed and solved iteratively one after the other. The solution obtained from the preceding system is always considered as the starting value when solving the following system. The systems used differ first by the parameters that are subject to improvement, second by the photometric data used, third by the weights, and finally by the damping of the iteration [see Table 1; for more details see Degünther (1997)]. In this way, we always find physically meaningful starting values close to the final solution. Using these values, Eq. (4) can be solved successfully; that is, the optical properties minimizing the sum in Eq. (5) are found.

3. Verification of the method

Any mathematical inversion of measured data has to be checked with regard to several aspects.

1) There is no really practicable general procedure to determine uniquely the solution of a nonlinear inversion problem of our kind (Menke 1989). Therefore we used calculated photometric data based on the physical model as input to the mathematical inversion and checked if the procedure in total is capable of finding the ''true'' optical properties of the particles with sufficient accuracy (see section 3a).
2) It has to be investigated whether or not all calculated and measured photometric data agree with sufficient accuracy (see section 3b).
3) Like any other, our model describing the photometric data is necessarily an approximation. Furthermore there are unavoidable errors of measurement. Disagreement between model results and measurements arising from these facts may cause, even if they are very small, large errors of the inversion results (Twomey 1977). Additionally the optical properties of the particles on the filter may be different from those of particles in the airborne state. Therefore the optical properties of atmospheric particles obtained from the mathematical inversion have to be compared with the results from independent measurements on airborne particles (see section 3c).
4) Finally it must be examined whether or not the total errors of the results are small enough to be acceptable (see section 3d).

If our method should fail one or more of these tests, its results would be worthless.

a. Mathematical check of the inversion procedure

For the mathematical reliability test of the inversion procedure about 50 different combinations of optical properties of the filter and the particles were chosen. The combinations are representative of the observed variabilities of these properties. From each combination the normalized signals and fluxes for the particle-free and particle-loaded filter were calculated using the physical model [Eqs. (1) and (2)]. These calculated photometric data were treated like measurements and the inversion procedure applied to them. If the procedure works properly, its results must come close to the optical properties from which the photometric data were calculated.

The outcomes of the mathematical check are as follows.

1) The larger the optical thickness τ of the particle layer sampled on the Nuclepore filter, the smaller are the differences between the inversion results and the true optical properties of the particles. For example, at $\tau = 0.5$ the difference ranges from 10% to 20% in the case of the extinction coefficient and from 3% to 8% in the case of the single scattering albedo. At $\tau = 0.9$ the differences range from 7% to 12% and from 2% to 5%, respectively. For $\tau = 1.3$ the differences are between 2% and 6% and less than 2%, respectively. It is illustrated, in Fig. 5, that for the largest values of τ the resulting phase function of the particles is most exact.
2) The larger the single scattering albedo of the particles, the better agree the calculated and the true val-

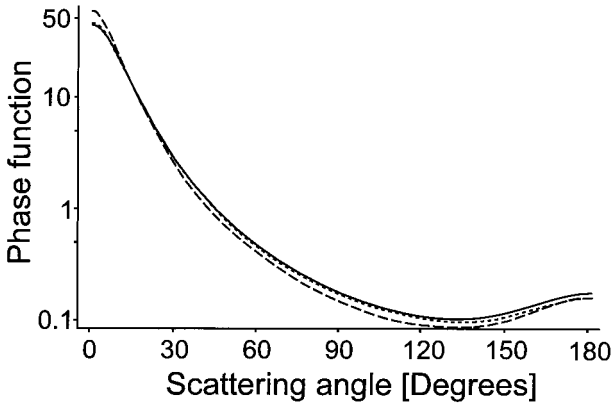

FIG. 5. Influence of the vertical optical thickness of the particle layer on the filter on the determination of the phase function. While for small τ ($\tau = 0.5$, dashed curve) one finds deviations between the real phase function (solid curve) and the result from our new inversion method, a greater τ ($\tau = 1.3$, dotted curve) leads to a nearly perfect coincidence between inversion result and reality.

ues of the particles' single scattering albedo and phase function.

Summarizing, the mathematical check can be regarded as passed as long as the vertical optical thickness of the particle layer collected on the filter is not smaller than 0.5. If $0.5 \leq \tau < 0.9$, the results of the inversion can be used, but errors up to 20% have to be accepted. For $\tau \geq 0.9$ the errors are small. Normally such particle layers can be collected on the filter without any problems.

b. Accuracy of calculated radiation fluxes

In this section the agreement between the calculated and measured radiation fluxes P_{0-30}–$P_{140-160}$ is investigated. Should this agreement be bad when the determined optical properties are similar to those obtained by independent measurements, obviously the physical model is not able to describe reality with sufficient accuracy. The realistic optical properties would be nothing but a lucky shot and deserve no trust. Only if the comparison yields no or only small differences between calculation and measurement, may the inversion results be accepted.

For the check, the calculated and measured radiation fluxes from 22 particle samples (see section 4) were compared. The relative deviations between calculated and measured radiation fluxes are less than 5% for P_{0-30}, $P_{110-120}$, and $P_{120-140}$; less than 3.5% (in 18 cases less than 2%) for P_{30-70}; and less than 3.2% (in 14 cases less than 2%) for $P_{140-160}$. These deviations are in the order of the experimental errors (see section 3d).

From this comparison the following conclusion may be drawn: the physical model describing the signals and fluxes is of the required accuracy. Consequently, if the inversion results are similar to the results from independent measurements on airborne particles, this happens not by chance, since our inversion procedure is able to find the true solution of Eq. (4) or at least a solution close to it.

c. Comparison of the new results with results taken from airborne particles and with results of a former inversion method

The next step necessary to accept the inversion results is to check if they are in accordance with results from independent measurements on airborne particles. Because the particles' extinction and absorption coefficients show temporal and spatial variabilities in the atmosphere of more than two orders of magnitude, it is always possible to find measurements in literature coinciding with our own inversion results. A comparison only makes sense if the particle sample under consideration is collected simultaneously at the same site at which the independent measurement takes place. Under these circumstances the extinction and absorption coefficients obtained by Hänel's inversion method (1994) were compared with measurements on airborne particles (Hänel 1987; Hänel and Hillenbrand 1989; Uhlig and von Hoyningen-Huene 1993; Uhlig et al. 1994). The results agreed within the error bars. The extinction and absorption coefficients determined with Hänel's inversion method are nearly identical with those obtained by our new developed method (mean differences 0.2% and 2.2%, respectively). Therefore, the mentioned excellent coincidence is valid not only for Hänel's results but also for the results presented here. For a more detailed comparison of the results of the present and Hänel's inversion method see Table 2.

To check the inverted phase functions of the particles, they are compared with nephelometric data. Many measurements of this kind are available for particles from single substances as, for example, quartz, MgO, NaCl, and ammonium sulfate (Holland and Gagne 1970; Perry et al. 1978; Kuik et al. 1991; Combet and Lamy 1995),

TABLE 2. Differences between results of this paper and results of the former inversion method by Hänel.

	Extinction coefficient	Scattering coefficient	Absorption coefficient	Single scattering albedo	Asymmetry parameter
Minimum error (%)	0.0	0.2	0.4	0.0	0.1
Mean error (%)	0.2	1.1	2.2	0.9	1.8
Maximum error (%)	1.1	3.5	8.1*	2.8	8.7*

* Only two numbers larger than 5%.

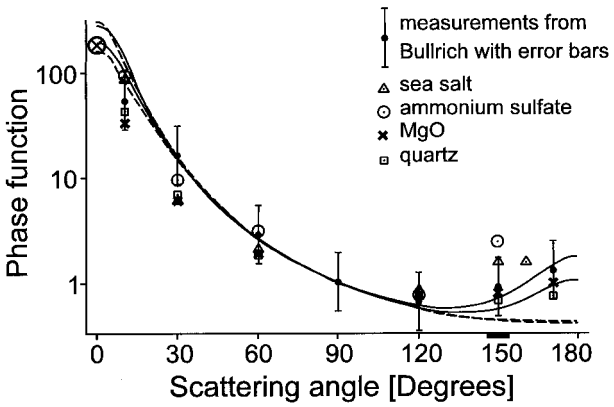

FIG. 6. Comparison of particles' phase functions. The two solid curves enclose the range comprising the phase functions obtained from our new inversion method for 22 different particle samples. Correspondingly, the dashed curves illustrate the variability of phase functions obtained for the same 22 particle samples, but from the inversion procedure by Hänel (1994). The different symbols indicate nephelometer measurements on airborne particles. Results are shown for atmospheric particles (Bullrich measurements) as well as for some of their constituents. The × in the circle marks atmospheric particles' phase function for scattering angle 0°. It is assessed from Bullrich's measurements, as described in section 3c. Due to better comparability all results are normalized to 1 at scattering angle 90°.

but only a very few (e.g., Bullrich 1960) for airborne atmospheric particles.

The results by Bullrich (1960) are given in Fig. 6 together with the phase function obtained by the new inversion method. Bullrich's values at the smallest scattering angle (10°) have to be considered cautiously: both the detector and the scattering volume have finite extensions. Hence, the radiation registered by the detector comes from different scattering angles, but the signal is assigned to one mean scattering angle. This leads to the largest possible errors at the smallest scattering angles. The scattered radiation could not be measured at scattering angles less than 10°. However, to get an idea of the phase function for small scattering angles, its value for $\psi = 0°$ is assessed as follows. In the range of forward scattering (scattering angle $\psi \leq 30°–40°$), the measured phase functions of different ensembles of poly- or monodisperse particles with irregular shape are similar to those derived from Mie theory for corresponding ensembles of volume or area equivalent spheres (Zerull 1976; Pollack and Cuzzi 1980). These observations agree with electromagnetic theory, which states that the phase function for small scattering angles should be nearly independent of the particles' shape, structure, and composition (Bohren and Huffman 1983). Considering these facts, the value of the phase function for $\psi = 0°$ can be assessed from the reliably measurable phase function between $\psi = 20°$ and $\psi = 40°$. Applying this assessment to the results of Bullrich leads to a value of the phase function for $\psi = 0°$, which is marked in Fig. 6 by a cross in a circle.

The agreement between the phase functions from our 22 particle samples and Bullrich's results from airborne atmospheric particles, including the assessed value for $\psi = 0°$, is convincing. Thus, our inversion method is capable of yielding realistic phase functions of atmospheric particles.

The measured phase functions for particles of one substance, which are added to Fig. 6, are less suitable for comparison with our inversion results, because the atmospheric particles contributing most to the phase function in the solar range of wavelengths are normally mixtures of different substances. Thus, these results are only rough approximations to atmospheric conditions.

d. Experimental errors of the results

Our photometric data have random errors that lead to uncertainties in the inversion results. In this section these uncertainties are quantified.

The random error of the photometric measurements is divided into two parts. The first part is caused by short-time instabilities of the lamp and the detector. It can be different for each signal and yields errors of about 0.5% for $P_{0–30}$, $P_{30–70}$, $P_{120–140}$, and $P_{140–160}$ and up to 1.2% for $P_{110–120}$. The effects of these errors on the inversion results are calculated using the Gaussian error propagation formula and are given in the second row of Table 3. They are small, especially for the parameters determining the phase function. The maximum uncertainties of σ_E, σ_A, and σ_S are smaller than 5%. The second part of the random error is caused by longtime

TABLE 3. Percentage errors of the inversion results due to fluctuations of the lamp. Partly, the errors depend on the vertical optical thickness τ of the particle layer on the filter. In this case there are two values given in one field. The value in parentheses is representative for a τ of approximately 0.6, while the one without parentheses is valid for a τ of at least 0.9. Parameters σ_E, σ_S, and σ_A are extinction, scattering, and absorption coefficients. The value σ_S/σ_E is the single scattering albedo; n and k are real, imaginary part of the apparent refractive index; α_S is the apparent soot content in percent of volume of the particulate material; g_1, g_2, and b are parameters of the phase function [Eq. (3)]; and g is asymmetry parameter of the phase function after Eq. (3).

Optical property	σ_E	σ_S	σ_A	σ_S/σ_E	g_1	g_2	b	n	k	α_S
Error caused by										
short-time instabilities	3–4	3–4	3–5	0.5–2	2.5	0.5	0.1	<0.5	2–10	1–10
Error caused by	4–12	5–13	1–7	<2					1–10	1–12
longtime instabilities	(22)	(23)	(10)	(5.5)	1	3	<0.25	<1.5	(27)	(30)
Maximum error	12.6	13.6	8.4	<2.9					14.1	15.6
	(22.4)	(23.3)	(11.2)	(5.9)	2.7	3	<0.3	<1.6	(28.8)	(31.6)

fluctuations of the lamp. It is smaller than 2.5% for all five radiation fluxes. The effect of this second error type on the inversion results is calculated as follows. From measured normalized radiation fluxes the optical properties of the particles are determined. Afterward, the fluxes are changed artificially by 2.5% and new values of the optical properties are calculated. The deviations of the new results from those obtained from the unchanged fluxes are the maximum uncertainties that can be caused by a longtime instability of the lamp. These uncertainties partly depend on the vertical optical thickness of the particle layer on the filter. If τ is not too small ($\tau \geq 0.9$), the uncertainties of σ_E, σ_A, and σ_S do not exceed 13% (Table 3, third row). The uncertainties of the asymmetry parameters g_1 and g_2 and the weight b are very small, 1%, 3%, and $<0.25\%$, respectively. Keeping in mind that b is always larger than about 0.985 (Table 4), the uncertainty of the weight $(1 - b)$ of the second Henyey–Greenstein function [see Eq. (3)] may reach 20%.

The maximum experimental errors of the inversion results are calculated as follows. The errors caused by the two parts of the random fluctuations of the lamp are squared and summed up. The square root of this sum is the maximum experimental error being listed in the fourth row of Table 3. It is smaller than about 13% (8%) for the extinction (absorption) coefficient, about 3% for the single scattering albedo. In the case of the phase function it changes from about 3% for the forward scattering to about 20% for the backward scattering. These numbers are valid for an optical thickness of the particles larger than about 0.9.

4. Results and discussion

Fourteen samples were collected in an urban area (city of Frankfurt am Main, Germany, 15 m above ground) and eight in a rural environment (about 20 km northwest of the city of Frankfurt am Main on top of the mountain Kleiner Feldberg about 830 m above mean sea level, Taunus, Germany, 7 m above ground). In total the samples were taken from all main airmass types observed in central Germany: continental and maritime polar air in September 1995 and March 1996 and continental and maritime tropical air in October 1995 and February 1996. One sample in September 1995 was taken from continental air with a long residence time in central Europe because of low wind speeds.

A summary of our main results is presented in Table 4 and Fig. 6 showing the subsequent features.

1) The data from February and March 1996 show that all attenuation coefficients (σ_E, σ_S, and σ_A) decrease considerably with height from the station in the city of Frankfurt am Main to the station on Kleiner Feldberg. Similar decreases with height along the slope of a mountain area or in the atmospheric boundary layer already have been observed in northern Italy and western Europe (Hänel 1994; Hänel 1998).

TABLE 4. Spectral mean values of the optical properties of dry atmospheric particles for the solar radiation. The results can also be regarded as spectral values at the wavelength 0.7 μm. The symbols are like in Table 2. Superscript "I" denotes the parameters of the least asymmetric phase function and superscript "II" those of the most asymmetric phase function. The apparent complex refractive index and the apparent soot content are derived from σ_E and σ_A using the formulas given by Hänel (1988).

Location	Time period	Number of measurements		σ_S (10^{-4} m^{-1})	σ_A	σ_S/σ_E	Phase function				α_S (%)
			σ_E				$g_1/g_2/b$	g	n	k	
Frankfurt am Main	Sep 1995	4	Min	0.218	0.137	0.612	0.813/−0.670/0.9895[I]	0.797	1.542	0.0659	16.2
			Mean	0.321	0.171	0.647		0.801	1.570	0.102	25.0
			Max	0.476	0.238	0.693	0.819/−0.716/0.9938[II]	0.810	1.590	0.129	31.6
Kleiner Feldberg (Taunus)	Oct 1995	3	Min	0.125	0.0562	0.677	0.792/−0.720/0.9921[I]	0.780	1.569	0.100	24.6
			Mean	0.164	0.0721	0.693		0.784	1.583	0.119	29.2
			Max	0.213	0.0865	0.712	0.811/−0.684/0.9856[II]	0.789	1.594	0.135	33.0
Frankfurt am Main	Feb–Mar 1996	10	Min	0.247	0.102	0.690	0.784/−0.673/0.9907[I]	0.770	1.506	0.0212	4.70
			Mean	0.820	0.246	0.757		0.780	1.522	0.0397	9.52
			Max	1.84	0.454	0.813	0.807/−0.663/0.9945[II]	0.799	1.544	0.0679	16.7
Kleiner Feldberg (Taunus)	Feb–Mar 1996	5	Min	0.115	0.0380	0.747	0.744/−0.720/0.9976[I]	0.741	1.522	0.0408	9.81
			Mean	0.242	0.0663	0.776		0.774	1.535	0.0572	14.0
			Max	0.521	0.122	0.809	0.821/−0.692/0.9921[II]	0.809	1.548	0.0726	17.9

2) The imaginary part of apparent refractive index and the soot content of the particles sampled during February and March 1996 are considerably lower than of the particles taken during September and October 1995. The single scattering albedo shows the opposite trend. This feature can be explained by the low inversions of temperature prevailing during the sampling periods in September and October 1995. During such situations the regionally emitted soot (traffic, industrial activities, and also some space heating) remains in the atmospheric boundary layer.
3) In the paper by Hänel (1994) the range of the single scattering albedo is 0.586–0.993, whereas in our investigation it ranges only between 0.612 and 0.813. This is explained as follows. In the earlier paper results from 181 samples taken during all seasons and at various locations in Germany and Italy were given. In the present paper we deal with 22 samples taken from September 1995 until March 1996 in and nearby Frankfurt am Main. Thus, all of the 22 samples are from one region and from a limited period of time, and the smaller variability of the single scattering albedo found in the present studies appears to be likely.
4) The asymmetry parameter of the phase function ranges from 0.74 to 0.81 and thus shows little variability with the weather situation or aerosol type. The ratio between backward and total scattering (ratio of the integrals of the phase function from 90° to 180° and from 0° to 180° of the scattering angle) varies between 0.050 and 0.071, that is, much more than the asymmetry parameter. However, in the present stage of research no systematic relationships between these parameters on the one hand and weather situation or aerosol type on the other hand have been found.
5) In general, dry atmospheric particles (which we are dealing with) are mixtures of different substances; that is, they are inhomogeneous, irregular, and absorbing. It is known from microwave analog measurements (e.g., Zerull 1976; Zerull et al. 1980) that phase functions of irregular absorbing particles clearly show a slight increase toward backscattering. In contrary, considering the same scattering angle range, the phase function of absorbing spheres of the same volume and material is decreasing. Taking into account these results, the slight increase of the investigated particles' phase function toward backscattering, as shown in Fig. 6, had to be expected. In our phase function approximation [Eq. (3)] the extent of this slight increase is mainly determined by the weight $(1 - b)$ of the Henyey–Greenstein function $\varphi_{\mathrm{HG}}(\psi, g_2)$ ranging between 0.0024 and 0.015, and not by the asymmetry parameter g_2. Both, $(1 - b)$ and g_2, do not depend on the particles' soot content.
6) It is of interest to compare the asymmetry parameter of our phase function [Eq. (3)] with the asymmetry parameter by Hänel (1994), who used only one Henyey–Greenstein function to approximate the phase function of scattering of dry atmospheric particles. The results of this comparison are the following. 1) The mean deviation between both asymmetry parameters is -0.002, which is negligible compared to the errors. 2) The absolute values of the individual deviations are in all cases smaller than the errors, in the majority small compared to the errors. This means that the Henyey–Greenstein asymmetry parameter by Hänel should describe realistically the phase function asymmetry of dry or nearly dry atmospheric particles. Consequently, approximating the phase function with only one Henyey–Greenstein function is suitable for climate modeling purposes.
7) A comparison of our results for the phase function and the corresponding results by Hänel is shown in Fig. 6. It is obvious that the one-parameter Henyey–Greenstein function convincingly approximates measurements on airborne particles within the scattering angle range 0° to about 130°. Out of this range the deviation between this approximation on the one hand and the measurements and our results on the other hand increases with scattering angle. The implications of such a deviation for aerosol remote sensing were investigated by Mishchenko et al. (1995). It was found, that the errors in retrieved aerosol optical depth due to incorrect description of particles' backscattering easily may exceed 100%, depending on satellite's zenith angle. Hence, just because of our phase function improvement it is now possible to apply the results of our new method in remote sensing applications, too.

5. Summary

A new inversion method has been developed yielding from one sample of atmospheric particles all optical properties necessary for radiative transfer calculations. These optical properties are the extinction and the absorption coefficients as well as the phase function. Compared to an earlier investigation of one of the authors (G.H.), the inverted phase function could be improved considerably, now describing also the backward scattering of radiation realistically. The new phase function is a three-parameter combination of two Henyey–Greenstein functions.

Summing up the mathematical and experimental errors of the method (from sections 3a and 3d) for an optical thickness of the particle layer sampled on the filter larger than 0.9, we get maximum possible errors for the entire method of about 18% (13%) for the extinction (absorption) coefficient and of about 10% (30%) for the part of the phase function describing mainly the forward (backward) scattering. These errors are sufficiently small for all optical properties. Thus, our inversion method yields results that allow investigation of all kinds of atmospheric radiative transfer problems

being affected by particles, including remote sensing of the atmosphere using lidar or satellites.

Acknowledgments. The financial support by the Deutsches Zentrum für Luft- und Raumfahrt (DLR) is gratefully acknowledged.

REFERENCES

Blanchet, J.-P., 1982: Application of the Chandrasekhar mean to aerosol optical parameters. *Atmos.–Ocean,* **20,** 189–206.

Bohren, C. F., and D. R. Huffman, 1983: *Absorption and Scattering of Light by Small Particles.* Wiley & Sons, 530 pp.

——, and S. B. Singham, 1991: Backscattering by nonspherical particles: A review of methods and suggested new approaches. *J. Geophys. Res.,* **96,** 5269–5277.

Bullrich, K., 1960: Streulichtmessungen in Dunst und Nebel. *Meteor. Rundsch.,* **13,** 21–29.

Chandrasekhar, S., 1960: *Radiative Transfer*. 2d ed. Dover, 393 pp.

Combet, P., and P. L. Lamy, 1995: Laboratory measurements of light scattering by dust particles. *Adv. Space Res.,* **15,** 65–68.

Degünther, M., 1997: Gleichzeitige Bestimmung aller optischen Eigenschaften atmosphärischer Partikeln durch mathematische Inversion photometrischer Messungen: Verwendung einer realitätsnah parametrisierten Phasenfunktion. Ph.D. dissertation, University Frankfurt am Main, 138 pp. [Available from Johann Wolfgang Goeth-Universität, Senckenberganlage 31, P. O. Box 11 19 32, 60054 Frankfurt, Germany.]

Durkee, P. A., F. Pfeil, E. Frost, and R. Shema, 1991: Global analysis of aerosol particle characteristics. *Atmos. Environ.,* **25A,** 2457–2471.

Flowers, E. C., R. A. McCormick, and K. R. Kurfis, 1969: Atmospheric turbidity over the United States. *J. Appl. Meteor.,* **8,** 955–962.

Hänel, G., 1976: The properties of atmospheric aerosol particles as functions of the relative humidity at thermodynamic equilibrium with surrounding moist air. *Advances in Geophysics,* Vol. 16, Academic Press, 73–188.

——, 1987: Radiation budget of the boundary layer. Part II: Simultaneous measurement of mean solar volume absorption and extinction coefficients of particles. *Contrib. Atmos. Phys.,* **60,** 241–247.

——, 1988: Single scattering albedo, asymmetry parameter, apparent refractive index, and apparent soot content of dry atmospheric particles. *Appl. Opt.,* **27,** 2287–2295.

——, 1994: Optical properties of atmospheric particles: Complete parameter sets obtained through polar photometry and an improved inversion technique. *Appl. Opt.,* **33,** 7187–7199.

——, 1998: Vertical profiles of the scattering coefficient of dry atmospheric particles over Europe normalized to air at standard temperature and pressure. *Atmos. Environ.,* **32,** 1743–1755.

——, and C. Hillenbrand, 1989: Calorimetric measurement of optical absorption. *Appl. Opt.,* **28,** 510–516.

Hansen, J. E., 1969: Radiative transfer by doubling very thin layers. *Astrophys. J.,* **155,** 565–573.

——, 1971: Multiple scattering of polarized light in planetary atmospheres. Part II: Sunlight reflected by terrestrial water clouds. *J. Atmos. Sci.,* **28,** 1400–1426.

Hill, S. C., A. C. Hill, and P. W. Barber, 1984: Light scattering by size/shape distributions of soil particles and spheroids. *Appl. Opt.,* **23,** 1025–1031.

Holland, A. C., and G. Gagne, 1970: The scattering of polarized light by polydisperse systems of irregular particles. *Appl. Opt.,* **9,** 1113–1121.

Hovenier, J. W., 1971: Multiple scattering of polarized light in planetary atmospheres. *Astron. Astrophys.,* **13,** 7–29.

Irvine, W. M., 1965: Multiple light scattering by large particles. *Astrophys. J.,* **142,** 1563–1575.

Kattawar, G. W., 1975: A three parameter analytic phase function for multiple scattering calculations. *J. Quant. Spectrosc. Radiat. Transfer,* **15,** 839–849.

Kuik, F., P. Stammes, and J. W. Hovenier, 1991: Experimental determinations of scattering matrices of water droplets and quartz particles. *Appl. Opt.,* **30,** 4872–4881.

Levin, Z., and J. D. Lindberg, 1979: Size distribution, chemical composition, and optical properties of urban and desert aerosol in Israel. *J. Geophys. Res.,* **84,** 6941–6950.

Liou, K. N., and Y. Takano, 1994: Light scattering by nonspherical particles: Remote sensing and climate impactions. *Atmos. Res.,* **31,** 271–298.

McGuire, A. F., and B. W. Hapke, 1995: An experimental study of light scattering by large, irregular particles. *Icarus,* **113,** 134–155.

Menke, W., 1989: *Geophysical Data Analysis: Discrete Inversion Theory*. Academic Press, 289 pp.

Mishchenko, M. I., A. A. Lacis, B. E. Carlson, and L. D. Travis, 1995: Nonsphericity of dust-like tropospheric aerosols: Implications for aerosol remote sensing and climate modeling. *Geophys. Res. Lett.,* **22,** 1077–1080.

Patterson, E. M., 1981: Optical properties of the crustal aerosol: Relation to chemical and physical characteristics. *J. Geophys. Res.,* **86,** 3236–3246.

Perry, R. J., A. J. Hunt, and D. R. Huffman, 1978: Experimental determinations of Mueller scattering matrices for nonspherical particles. *Appl. Opt.,* **17,** 2700–2710.

Pollack, J. B., and J. N. Cuzzi, 1980: Scattering by nonspherical particles of size comparable to a wavelength: A new semi-empirical theory and its application to tropospheric aerosols. *J. Atmos. Sci.,* **37,** 868–881.

Press, W. H., B. P. Flannery, S. A. Teukolsky, and W. T. Vetterling, 1992: *Numerical Recipes.* 2d ed. Cambridge University Press, 963 pp.

Purcell, E. M., and C. R. Pennypacker, 1973: Scattering and absorption of light by nonspherical dielectric grains. *Astrophys. J.,* **186,** 705–714.

Schuerman, D. W., R. T. Wang, B. Å. S. Gustafson, and R. W. Schaefer, 1981: Systematic studies of light scattering. 1: Particle shape. *Appl. Opt.,* **20,** 4039–4050.

Shaw, G. E., 1980: Transport of Asian desert aerosol to the Hawaiian Islands. *J. Appl. Meteor.,* **19,** 1254–1259.

Spurný, K., 1965–66: Membranfilter in der Aerosologie II. Filtrationsmechanismen bei Membranfiltern. *Z. Biol. Aerosol-Forsch.,* **12–13,** 1–56.

Twomey, S., 1977: *Introduction to the Mathematics of Inversion in Remote Sensing and Indirect Measurements.* Elsevier, 243 pp.

Uhlig, E. M., and W. von Hoyningen-Huene, 1993: Correlation of the atmospheric extinction coefficient with the concentration of particulate matter for measurements in a polluted urban area. *Atmos. Res.,* **30,** 181–195.

——, M. Stettler, and W. von Hoyningen-Huene, 1994: Experimental studies on the variability of the extinction coefficient by different air masses. *Atmos. Environ.,* **28,** 811–814.

van de Hulst, H. C., 1980: *Multiple Light Scattering.* Vols. 1 and 2. Academic Press, 739 pp.

von Hoyningen-Huene, W., and A. Raabe, 1987: Maritime and continental air mass differences in optical aerosol extinction data. *Contrib. Atmos. Phys.,* **60,** 81–87.

Wang, M., and H. R. Gordon, 1993: Retrieval of the columnar aerosol phase function and single scattering albedo from sky radiance over the ocean-simulations. *Appl. Opt.,* **32,** 4598–4609.

Yeh, C., and K. K. Mei, 1980: On the scattering from arbitrarily shaped inhomogeneous particles—Exact solution. *Light Scattering by Irregular Shaped Particles,* D. W Schuerman, Ed., Plenum, 201–206.

Zerull, R. H., 1976: Scattering measurements of dielectric particles and absorbing nonspherical particles. *Contrib. Atmos. Phys.,* **49,** 168–188.

——, R. H. Giese, S. Schwill, and K. Weiss, 1980: Scattering by particles of non-spherical shape. *Light Scattering by Irregular Shaped Particles,* D. W. Schuerman, Ed., Plenum, 273–282.